

Article

Chemical Interaction between the $\text{Sr}_4\text{Al}_6\text{O}_{12}\text{SO}_4$ Ceramic Substrate and Al–Si Alloys

José Amparo Rodríguez-García ¹, Carlos Adrián Calles-Arriaga ¹, Ricardo Daniel López-García ²,
José Adalberto Castillo-Robles ¹ and Enrique Rocha-Rangel ^{1,*}

¹ Research Department, Universidad Politécnica de Victoria, Av. Nuevas Tecnologías 5902, Parque Científico y Tecnológico de Tamaulipas, Cd. Victoria 87138, Tamaulipas, Mexico; jrodriguez@upv.edu.mx (J.A.R.-G.); ccallesa@upv.edu.mx (C.A.C.-A.); jcastillor@upv.edu.mx (J.A.C.-R.)

² Mechanical Department, Tecnológico Nacional de México, Instituto Tecnológico de Cd. Victoria, Blvd. Emilio Poster Gil 1301, Cd. Victoria 87010, Tamaulipas, Mexico; ricardo.lg@cdvictoria.tecnm.mx

* Correspondence: erochar@upv.edu.mx

Abstract: Samples of $\text{Sr}_4\text{Al}_6\text{O}_{12}\text{SO}_4$ are obtained through a solid-state reaction of Al_2O_3 , SrSO_4 , and SrCO_3 . The samples are then made into 1 and 4 cm pellets by compacting them at 100MPa and sintering them at 1400 °C for 4 h. The compound is analyzed using X-ray diffraction. Static immersion and wettability tests are carried out to evaluate corrosion resistance in contact with Al–Si. Corrosion tests are conducted by immersing the samples at 800, 900, and 1000 °C for 24, 50, and 100 h, while wettability is studied at 900, 1000, and 1100 °C for 2 h. Afterwards, the samples are subject to metallographic preparation. The samples are then analyzed using optical microscopy, scanning electron microscopy, and image analysis. In general, reaction products consisting of alumina, spinel, oxides, and sulfates are found. The contact angles obtained are between 124° and 135°. It is concluded that the $\text{Sr}_4\text{Al}_6\text{O}_{12}\text{SO}_4$ ceramic substrate is resistant to corrosion by the Al–Si alloy because of the slight thickness of the reaction products found in the samples (73 μm), considering the severe conditions of the experiment: 1000 °C and 100 h of isothermal temperature. Furthermore, $\text{Sr}_4\text{Al}_6\text{O}_{12}\text{SO}_4$ is not wettable by Al–Si alloys. These results suggest that the ceramic substrate could be used in the refractory industry, possibly as an additive to commercial refractory ceramics. For future work, it is recommended to carry out the same study with the aluminum–magnesium alloy and as an additive in commercial refractory ceramics.

Keywords: solid-state reaction; static immersion; wettability; corrosion; aluminum alloys



Citation: Rodríguez-García, J.A.; Calles-Arriaga, C.A.; López-García, R.D.; Castillo-Robles, J.A.; Rocha-Rangel, E. Chemical Interaction between the $\text{Sr}_4\text{Al}_6\text{O}_{12}\text{SO}_4$ Ceramic Substrate and Al–Si Alloys. *Eng* **2024**, *5*, 461–476. <https://doi.org/10.3390/eng5010025>

Academic Editor: Tomasz Lipiński

Received: 28 November 2023

Revised: 22 February 2024

Accepted: 28 February 2024

Published: 5 March 2024



Copyright: © 2024 by the authors. Licensee MDPI, Basel, Switzerland. This article is an open access article distributed under the terms and conditions of the Creative Commons Attribution (CC BY) license (<https://creativecommons.org/licenses/by/4.0/>).

1. Introduction

The aluminum production industry, from scrap or directly from the mineral (bauxite), plays a significant role in the world economy and development. This relevance is largely due to the wide availability, ease of processing, and mechanical properties that allow it to have a wide range of applications, in some cases even comparable to steel [1–6]. For its production on an industrial scale, melting furnaces are used, which are mainly made up of refractory ceramics based on aluminosilicates (CRAS) due to their low cost, high availability, good mechanical properties, and resistance to corrosion and thermal shock [7–12]. However, this type of substrate presents a high corrosion rate in contact with liquid aluminum alloys (up to 6 mmh^{−1}) due to the strong reducing effect of aluminum on silicon, leading to the critical task of selecting refractories for melting furnaces [13–17].

Studies have been carried out as an alternative for enhancement where specific percentages of additives called “non-wettable agents” are added to the refractory material to improve corrosion resistance. Oliveira et al. doped CRAS-type samples with three types of oxide (MgO, CaO, and BaO) in order to investigate their influence on the reaction with liquid aluminum alloys. The experiments were carried out in a vacuum at temperatures of 750, 900, and 1050 °C for 4 h. The results showed that in the samples doped with barium

oxide, interfaces of approximately 300 μm thick were formed, while the samples doped with magnesium oxide presented reaction zones of approximately 650 μm thick, and in the samples doped with calcium oxide precipitates corresponding to $\beta\text{-Al}_2\text{CaSi}_2$ were formed, which functioned as a diffusion barrier between the ceramic and the liquid aluminum [6].

Allaire et al. investigated the effect of the presence of alkalis on the corrosion of CRAS-type samples by liquid aluminum. It was observed that the alumina layer reacted with sodium oxide (Na_2O), forming sodium aluminates (NaAlO_2), and by modifying the alumina layer, the volume of sodium aluminates increased, which promoted the formation of cracks and penetration of aluminum [18]. On the other hand, Ibarra et al. doped CRAS-type samples with strontium and barium sulfate, obtaining mullite- $\text{SrAl}_2\text{Si}_2\text{O}_8$ and mullite- $\text{BaAl}_2\text{Si}_2\text{O}_8$, respectively, to analyze the behavior in contact with liquid aluminum alloys. The reaction products formed were MgO and MgAl_2O_4 with a density of approximately 200 μm , which is lower than those formed in the samples without additives [19,20].

AdabiFiroozjaei et al. investigated the effect of AlPO_4 as an additive at 5% in CRAS-type samples. An improvement in corrosion resistance was observed due to the formation of corundum and gaseous P_2O_3 as reaction products, which prevented the advancement of the penetration of the aluminum alloy into the ceramic substrate [21]. Furthermore, complementary studies analyzed samples of $\text{BaAl}_2\text{Si}_2\text{O}_8$ in contact with aluminum alloys, developing an interdiffusion and substitution process to form alumina and spinel. The sample showed good corrosion resistance by presenting $\text{BaAl}_2\text{Si}_2\text{O}_8$ grains in the interfacial zone [22]. On the other hand, Rodríguez et al., in preliminary studies, stated that the strontium compound $\text{Sr}_4\text{Al}_6\text{O}_{12}\text{SO}_4$ presents good resistance to corrosion by Al-Si and Al-Mg alloys at 900 $^\circ\text{C}$ for 24 h, where the samples did not suffer penetration by the liquid metal [23].

Storozhenko et al. investigated the contact interaction between a hot-pressed chromium diboride ceramic material and an iron-based self-fluxing eutectic alloy (FeNiCrBSiC). The iron-based self-fluxing alloy was found to wet the chromium diboride substrate to form a contact angle $\theta = 12^\circ$. The structural and phase composition of the droplet and the contact interaction area in the FeNiCrBSiC-CrB₂ system were examined using electron microprobe analysis. In the wetting process, boron from the upper layer of the CrB₂ ceramic substrate diffused to the alloy area. The FeNiCrBSiC-CrB₂ system can be considered promising for the development of composite materials because intensive chemical interaction between the alloy and refractory components leads to additional superhard chromium-molybdenum borides and carboborides in the matrix, promoting greater wear resistance of thermal spray coatings of the composite material [24].

Xiaoyan et al. investigated the wetting and interfacial phenomena between superalloy melt and silica-based ceramic cores, taking into account the effect of ZrSiO_4 contents. They found that SiO_2 is the main component in the ceramic core, and the wetting angle increases in the initial 200 s to a peak value and then decreases to a constant value for the couples of ceramics containing 10 wt.%, 30 wt.%, and 50 wt.% ZrSiO_4 [25].

As can be seen, in all the previous cases, alkaline earth metals in different presentations were used as non-wettable agents to improve the refractory properties of the ceramic samples. This is why the hypothesis arises of considering the strontium compound ($\text{Sr}_4\text{Al}_6\text{O}_{12}\text{SO}_4$) as an option to use as a coating for aluminum smelting furnaces due to the components that make it up, such as alumina (refractory material with a high melting point) and compounds of strontium that are considered compounds of high thermal resistivity in addition to being abundant materials in nature. The general objective is to study the chemical interaction between the ceramic substrate $\text{Sr}_4\text{Al}_6\text{O}_{12}\text{SO}_4$ and the aluminum-silicon alloy through static immersion and wettability tests, determining its feasibility in the refractory industry.

2. Materials and Methods

2.1. Synthesis of Study Samples

The reagents Al_2O_3 , SrCO_3 , and SrSO_4 , grade reactive, according to a proportion of 3:3:1 molar to form $\text{Sr}_4\text{Al}_6\text{O}_{12}\text{SO}_4$, were mixed. The mixture was homogenized in a plastic jar with acetone and alumina balls by spinning for 4 h. The mixture was dried at 60 °C for 24 h. After drying, the mixture was ground in a mortar to disintegrate agglomerates. Disk pellets of 1 and 4 cm in diameter were made by uniaxial pressing at 100 MPa and heat treated at 1400 °C with an isotherm of 4 h and a heating/cooling rate of 5 °C min⁻¹ [26]. A sample of the sintered disks was ground in a mortar (3 g into powder) for X-ray diffraction analysis (XRD) to determine their composition.

2.2. Static Immersion Test

To carry out the static immersion corrosion tests, disk pellets (1 cm in diameter) were fixed at the base of a high-alumina crucible, and pieces of the Al-Si alloy were subsequently placed. Aluminum alloy samples were subjected to spark chemical analysis to determine their composition. Subsequently, the crucible was placed inside a covered resistance muffle. The working conditions were the application of temperatures of 800, 900, and 1000 °C, with isotherms of 25, 50, and 100 h and a heating/cooling rate of 10 °C min⁻¹. For each working condition, five study samples were tested. At the end of the corrosion tests, the samples were cold mounted in epoxy resin, cross-sectioned, and polished with SiC grinding media from 80 to 1200 grit size using ethanol as a lubricant. Subsequently, 3, 1, and ¼ µm diamond paste were used for final polishing. Then, the samples were analyzed using optical microscopy (Nikon NA200, Cole Palmer, Dubuque, IA, USA) and scanning electron microscopy (Philips XL30/ESEM, Philips, Amsterdam, The Netherlands) to study the formed phases' morphology and corroborate their chemical composition using the energy-dispersive spectroscopy (EDS) technique.

2.3. Wettability Test

In the wettability tests using the static drop method, a high-temperature tubular furnace (Thermolyne 59300, Thermo Fisher Scientific, Waltham, MA, USA), which has an alumina tube 76 cm long by 6 cm in diameter, was used. Additionally, at the ends of the tube, the equipment has aluminum caps with a cooling system that maintains the temperature of the caps through a water pump. One of the covers is provided with a viewing window through which the behavior of the aluminum alloy on the ceramic samples (4 cm in diameter) was monitored using a video camera. In the experiments, a controlled argon atmosphere (ultra-high purity) was used with a flow rate of 0.005 m³ min⁻¹. Prior to the test, 1 cm³ cubes of the aluminum Al-Si alloy were prepared and polished using SiC grinding media from 80 to 1200 grit size to eliminate impurities and surface rust. Subsequently, they were immersed in a hydrochloric acid (HCl) solution and cleaned with ethanol just before being placed in the furnace. In the tubular furnace, a zirconia sponge was placed on an alumina boat to eliminate residual oxygen inside the furnace. Afterward, the aluminum alloy cube was placed on the ceramic substrate and in the furnace on an alumina base. The lids were placed to start the heat treatment, and the argon flow was released.

The working conditions were the application of temperatures of 900, 1000, and 1100 °C, with isotherms of 2 h and a heating/cooling rate of 15 °C min⁻¹. For each working condition, five study samples were tested. They were taken from images extracted every 10 min of the video recording. They were measured by drawing tangents between the alloy droplet and the ceramic samples on both sides of the droplet. At the end of the wettability tests, the samples were cold mounted in epoxy resin and cross-sectioned; polished SiC grinding media from 80 to 1200 grit size using ethanol were used as a lubricant. Subsequently, 3, 1, and ¼ µm of diamond paste were used for final polishing. Then, the samples were carbon coated and analyzed using scanning electron microscopy (Philips

XL30/ESEM) to study the formed phases' morphology and corroborate their chemical composition using the energy-dispersive spectroscopy (EDS) technique.

3. Results

3.1. Characterization of Materials

The results of the formation synthesis of the study samples are presented in Figure 1. It can be seen in the X-ray diffraction pattern that only intensities corresponding to the strontium compound $\text{Sr}_4\text{Al}_6\text{O}_{12}\text{SO}_4$ are recorded throughout the entire length of the analyzed samples. This means that the synthesis process used and reported in the literature was effective [23].

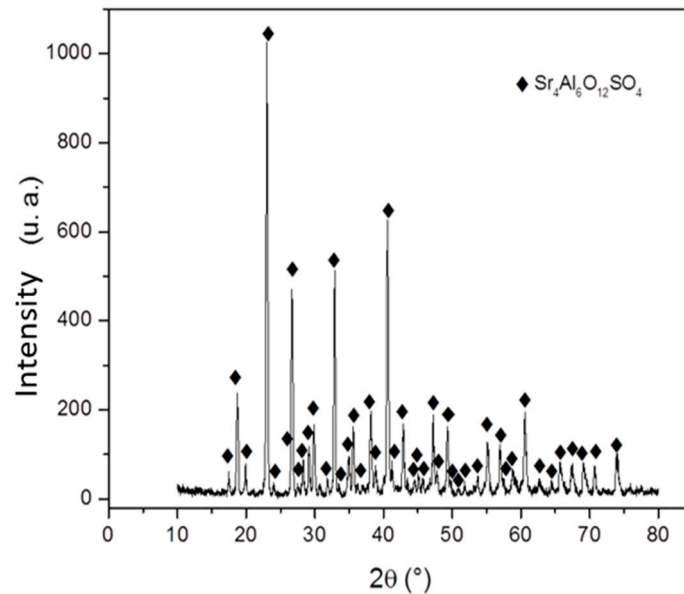


Figure 1. X-ray diffraction pattern of representative samples of the synthesis process of the strontium compound $\text{Sr}_4\text{Al}_6\text{O}_{12}\text{SO}_4$.

Table 1 shows the results of the spark chemical analysis of the composition of the aluminum alloy used in the static immersion and wettability tests.

Table 1. Chemical composition of aluminum alloy (Wt, %).

Aluminum Alloy	Si	Fe	Cu	Mn	Mg	Cr	Ni	Zn	Ti	Al
Al-Si	7.420	0.717	2.630	0.437	0.454	0.050	0.041	0.637	0.158	87.456

As can be seen, the alloy contains more than 7 wt% silicon as an alloying element. As reported in the literature, the content of this element considerably affects behavior in corrosive processes [19,27].

3.2. Static Immersion Test Results

Figure 2 presents micrographs of the study samples after static immersion tests in Al-Si alloys at 800 °C and isotherms of 25 h (A), 50 h (B), and 100 h (C) as experimental conditions.

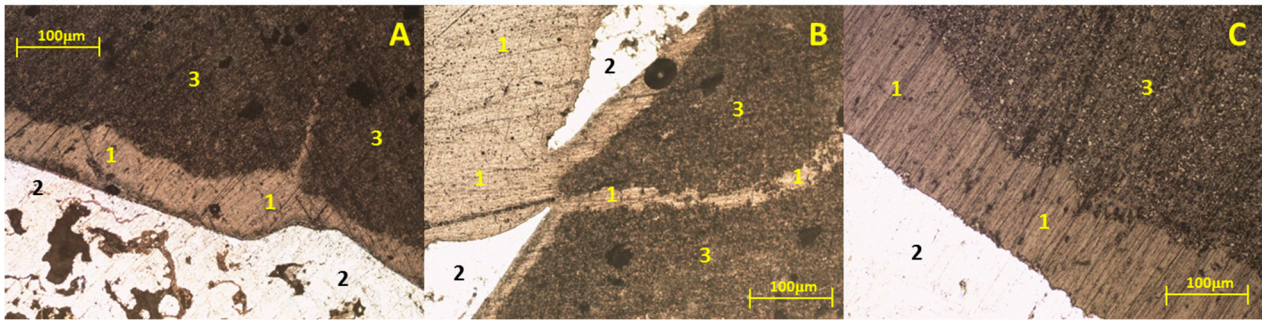


Figure 2. Micrographs of study samples after static immersion tests in Al-Si alloy at 800 °C and isotherms of 25 h (A), 50 h (B) and 100 h (C). 1: resin, 2: Al-Si alloy, and 3: $\text{Sr}_4\text{Al}_6\text{O}_{12}\text{SO}_4$.

It is worth mentioning that, due to the physical conditions of the study samples (low mechanical properties), the metallographic preparation was complicated, bringing with it, in some cases, the introduction of resin between areas of the study sample and the metal. It can be seen in the three micrographs that under these experimental conditions, there is no chemical interaction between the ceramic substrate $\text{Sr}_4\text{Al}_6\text{O}_{12}\text{SO}_4$ and the Al-Si alloy; that is, there was no formation of reaction products (analyzing the metal surface). Figure 3 presents micrographs of study samples after static immersion tests in Al-Si alloys at 900 °C and isotherms of 25 h (A), 50 h (B), and 100 h (C) as experimental conditions.

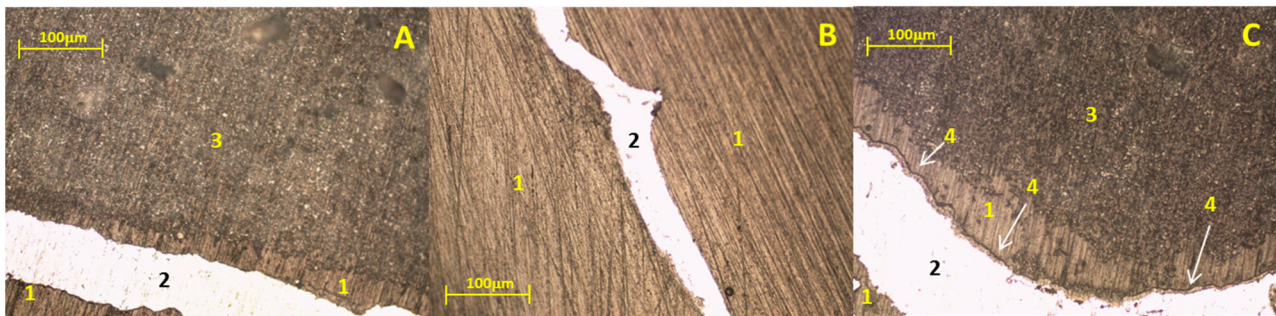


Figure 3. Micrographs of study samples after static immersion tests in Al-Si alloy at 900 °C and isotherms of 25 h (A), 50 h (B) and 100 h (C). 1: resin, 2: Al-Si alloy, 3: $\text{Sr}_4\text{Al}_6\text{O}_{12}\text{SO}_4$, and 4: reaction zone.

Micrographs A and B show no chemical interaction between the ceramic substrate $\text{Sr}_4\text{Al}_6\text{O}_{12}\text{SO}_4$ and the Al-Si alloy; that is, there was no formation of reaction products. However, a thin line of reaction products adhered to the metal surface in micrograph C can be seen. Due to the limitation of the characterization technique, it is impossible to determine the chemical composition of the registered reaction products to complement the results.

Figure 4 presents the SEM micrographs and EDS analysis of study samples after static immersion tests in Al-Si alloys at 900 °C and 100 h as experimental conditions. The micrograph presents the visual analysis of an area of the study sample, and the EDS spectra present the specific chemical analysis of different areas. According to the percentages of the registered chemical elements, the particles identified with the number 1 are related to the ceramic substrate $\text{Sr}_4\text{Al}_6\text{O}_{12}\text{SO}_4$, and the areas identified with numbers 2 and 3 correspond to the Al-Si alloy (one with higher purity than the other). In addition, reaction products are presented due to the chemical interaction between the ceramic substrate $\text{Sr}_4\text{Al}_6\text{O}_{12}\text{SO}_4$ and the Al-Si alloys, such as areas of spinels (MgAl_2O_4) identified with number 4 and intermetallics of the alloy (MgO) identified with number 5.

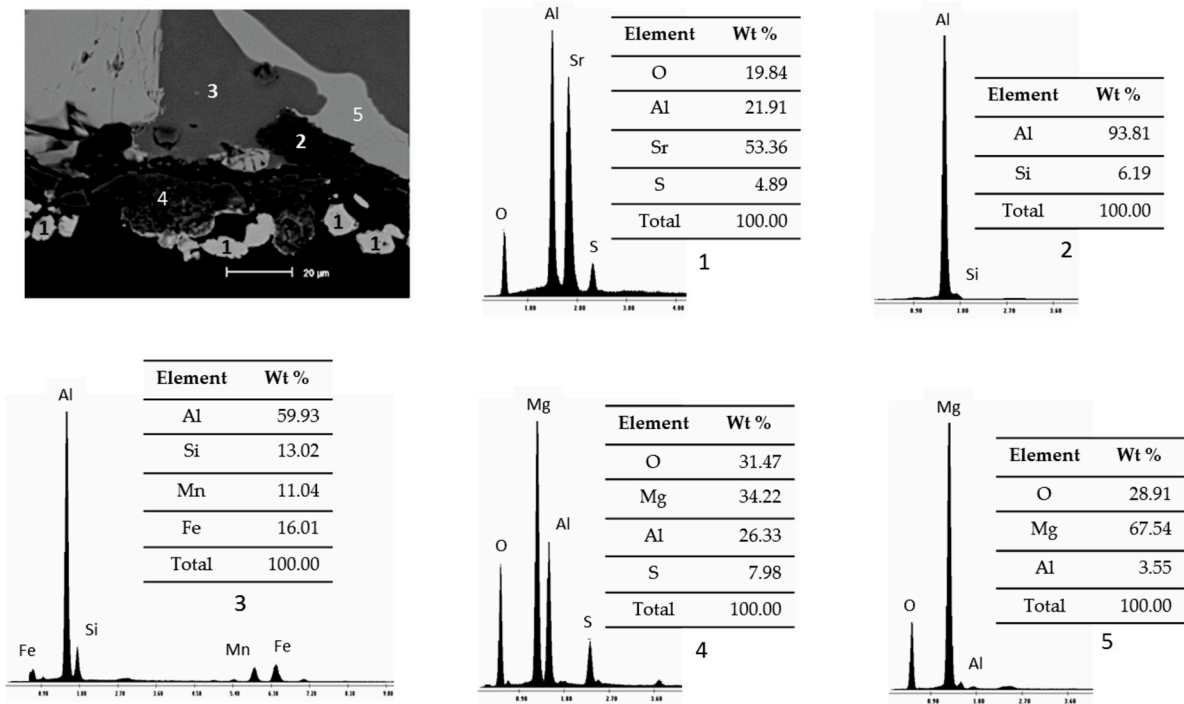


Figure 4. SEM micrograph and EDS spectra of study samples after static immersion tests in Al-Si alloy at 900 °C for 100 h as experimental conditions.

Figure 5 shows the mapping via chemical element (SEM) present in study samples after the static immersion test in Al-Si alloys at 900 °C for 100 h as experimental conditions.

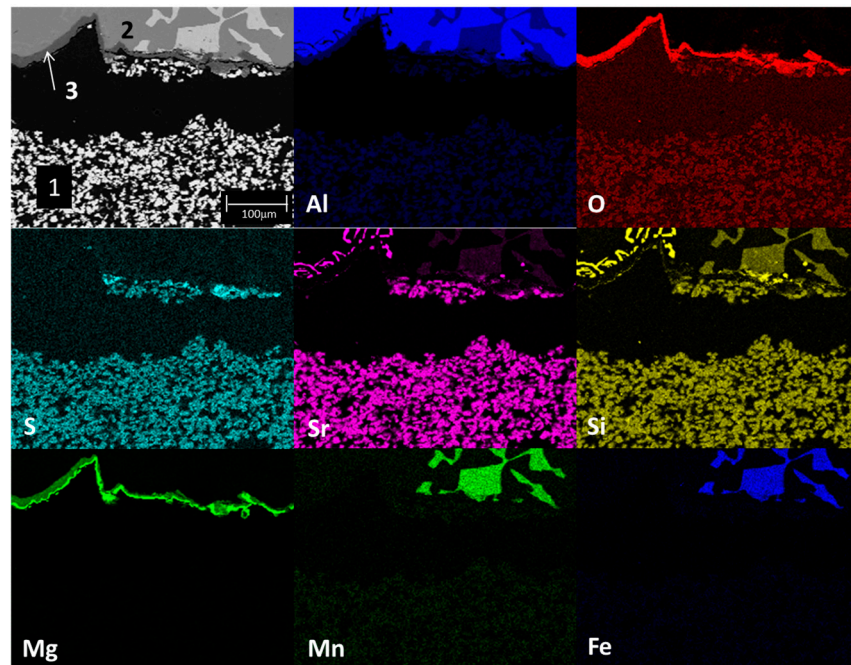


Figure 5. Mapping via chemical element present in study samples after static immersion tests in Al-Si alloy at 900 °C for 100 h as experimental conditions. 1: $\text{Sr}_4\text{Al}_6\text{O}_{12}\text{SO}_4$, 2: Al-Si alloy, and 3: reaction products.

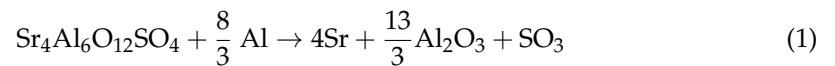
The main micrograph (upper left corner) presents the section of the study sample analyzed. Three main areas are observed: at the bottom, agglomerates of white particles (1); at the top, a solid section of mainly light-gray color (2); and attached to the bottom

of Section 2, a thin dark-gray line (3). According to the distribution of chemical elements, the area identified with the number 1 (light-colored agglomerates) corresponds to the ceramic substrate $\text{Sr}_4\text{Al}_6\text{O}_{12}\text{SO}_4$, the light-gray solid section identified with the number 2 corresponds to the Al–Si alloy (the light within Section 2 corresponds to manganese and iron intermetallics present in the alloy), and the thin dark-gray line identified with the number 3 corresponds to reaction products of the type spinel (MgAl_2O_4) and magnesium oxide (MgO).

This phenomenon, where magnesium diffuses to the metal–ceramic interface, has been reported in the literature, increasing its content in this area [20]. On the other hand, strontium diffusion from the ceramic substrate towards the metal alloy, silicon, manganese, and iron from the metal alloy towards the ceramic substrate is observed. The above results show the chemical interaction process between the ceramic substrate and the alloy in Al–Si alloys (corrosion).

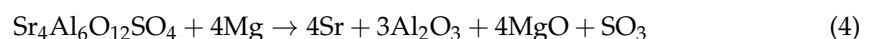
The mapping of iron and manganese elements shows the distribution of intermetallics within aluminum. Based on the results presented, two interaction mechanisms are proposed between the ceramic substrate $\text{Sr}_4\text{Al}_6\text{O}_{12}\text{SO}_4$ with Al–Si alloys (900 °C–100 h) to form reaction products:

Mechanism number 1



According to mechanism number 1, it can be said that ceramic substrate $\text{Sr}_4\text{Al}_6\text{O}_{12}\text{SO}_4$, upon contact with the Al–Si alloy at 900 °C and 100 h, decomposes into three parts: strontium (Sr), alumina (Al_2O_3), and trioxide sulfur (SO_3). At the same time, the magnesium present in the alloy (<1%) is oxidized, giving rise to magnesium oxide (MgO). Finally, alumina and magnesium oxide (products of reactions 1 and 2) react with each other to form spinel (MgAl_2O_4).

Mechanism number 2



According to mechanism number 2, it can be said that the ceramic substrate $\text{Sr}_4\text{Al}_6\text{O}_{12}\text{SO}_4$, upon contact with the Al–Si alloy at 900 °C and 100 h, decomposes into four parts: strontium (Sr), alumina (Al_2O_3), magnesium oxide (MgO), and sulfur trioxide (SO_3). At the same time, the magnesium from the alloy is oxidized and reacts with alumina to produce spinel (MgAl_2O_4). Figure 6 presents the micrographs of study samples after static immersion tests in Al–Si alloys at 1000 °C and isotherms of 25 h (A), 50 h (B), and 100 h (C) as experimental conditions.

In the micrograph identified with the letter A, it can be seen that there is no apparent chemical interaction between the ceramic substrate $\text{Sr}_4\text{Al}_6\text{O}_{12}\text{SO}_4$ and the Al–Si alloy. However, a thin dark line can be observed at the border of the ceramic substrate as if it were burned. In micrographs B and C, a thin line of reaction products can be seen at the boundary of the metallic phase, which increases in thickness as a function of exposure time. To complement the results, Figure 7 presents the SEM micrographs and EDS analysis of study samples after static immersion tests in Al–Si alloys at 1000 °C and 100 h as experimental conditions.

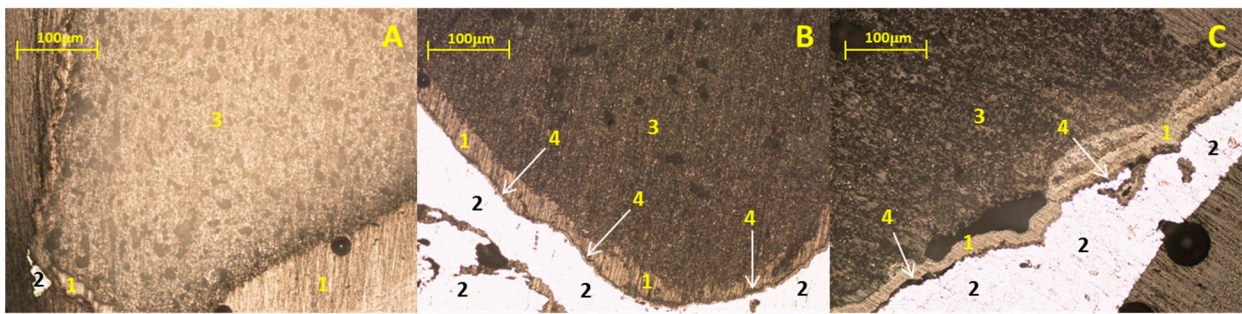


Figure 6. Micrographs of study samples after static immersion tests in Al-Si alloy at 1000 °C and isotherms of 25 h (A), 50 h (B) and 100 h (C). 1: resin, 2: Al-Si alloy, 3: $\text{Sr}_4\text{Al}_6\text{O}_{12}\text{SO}_4$, and 4: reaction zone.

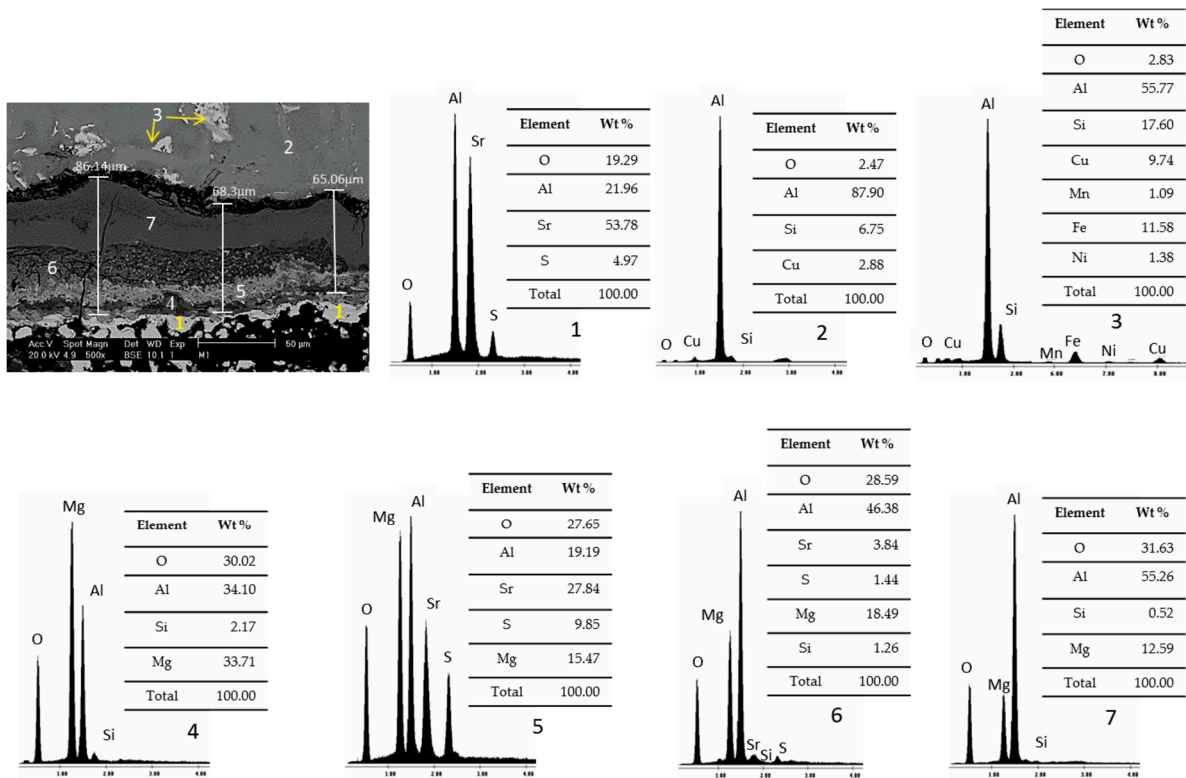


Figure 7. SEM micrograph and EDS spectra of study samples after static immersion tests in Al-Si alloy at 1000 °C for 100 h as experimental conditions.

According to the percentages of the registered chemical elements, the particles identified with the number 1 are related to the ceramic substrate $\text{Sr}_4\text{Al}_6\text{O}_{12}\text{SO}_4$, the area identified with the number 2 corresponds to the Al-Si alloy, and the particles identified with the number 3 correspond to mainly iron intermetallics. In addition, a corrosion layer is observed between the alloy and the ceramic substrate, with a mean value of 73 μm and a standard deviation of 29.74%, generating reaction products, mostly spinelas (MgAl_2O_4) in different magnesium concentrations (4, 5, 6, and 7). On the other hand, cracking can be observed through the corrosion layer due to the difference between the thermal expansion coefficients of the phases present [27]. Comparing these results with those found in the literature, they are very favorable since reaction zones are reported from 200 to 650 microns with a maximum working temperature of 1050 °C and 4 h of isotherm [6,18–20].

Figure 8 shows the mapping via the chemical element (SEM) present in the study sample after static immersion tests in Al-Si alloys at 1000 °C for 100 h as experimental conditions. The main micrograph (upper left corner) presents the study sample analyzed.

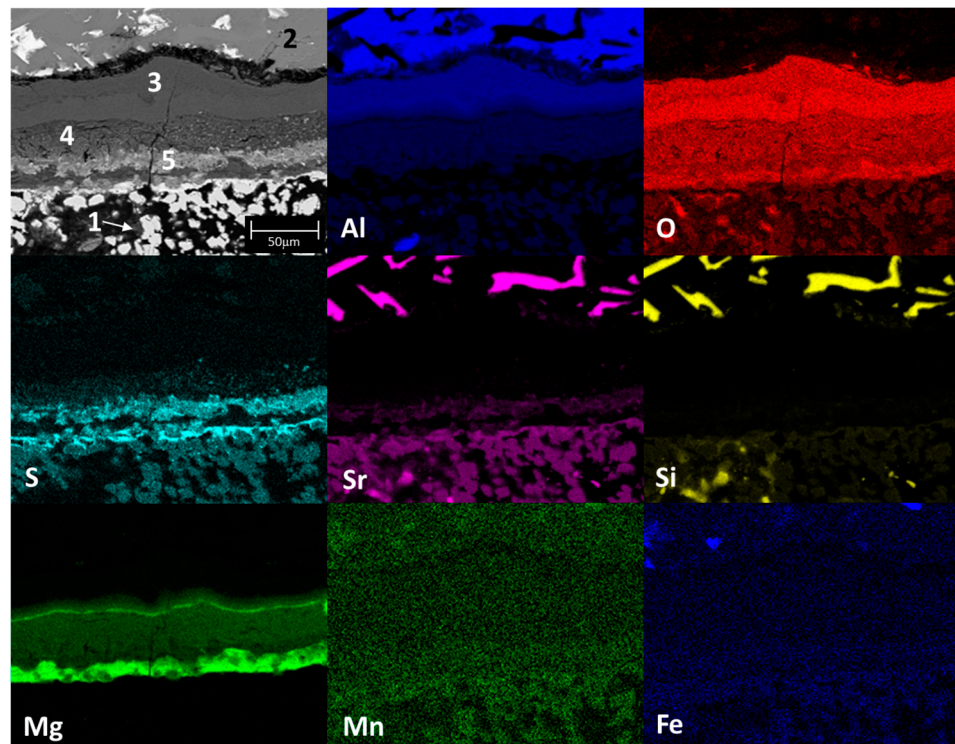


Figure 8. Mapping via chemical element present in the study sample after static immersion tests in Al-Si alloy at 1000 °C for 100 h as experimental conditions. 1: $\text{Sr}_4\text{Al}_6\text{O}_{12}\text{SO}_4$, 2: Al-Si alloy, and 3–5: reaction products.

Three main areas are observed: in the lower part, agglomerates of white particles (1); in the upper part, a solid section of light-gray color (2); and between these sections, there is a zone of reaction products. According to the distribution of chemical elements, the area identified with the number 1 (light-colored agglomerates) corresponds to the ceramic substrate $\text{Sr}_4\text{Al}_6\text{O}_{12}\text{SO}_4$; the light-gray solid section identified with the number 2 corresponds to the Al-Si alloy within the reaction zone; the alumina phase (Al_2O_3) is identified with the number 3; the spinel (MgAl_2O_4) and magnesium oxide (MgO) phases are identified with the number 4; and the presence of sulfates, possibly strontium (SrSO_4), is identified with the number 5. On the other hand, strontium diffusion from the ceramic substrate towards the metal alloy, silicon, manganese, and iron from the metal alloy towards the ceramic substrate is observed. This reaction results from the chemical interaction process between the ceramic substrate and the aluminum-silicon alloy (corrosion).

Based on the previous results, the following interaction mechanism is proposed between the ceramic substrate $\text{Sr}_4\text{Al}_6\text{O}_{12}\text{SO}_4$ and Al-Si alloys (1000 °C–100 h) to form reaction products:



According to the proposed mechanism, it can be said that sections of the ceramic substrate $\text{Sr}_4\text{Al}_6\text{O}_{12}\text{SO}_4$, upon contact with the Al-Si alloy at 1000 °C and 100 h, decompose into three parts: strontium (Sr), alumina (Al_2O_3), and strontium sulfate (SrSO_4). At the same time, the magnesium present in the alloy (<1%) is oxidized, giving rise to magnesium oxide (MgO). Alumina and magnesium oxide react to produce spinel (MgAl_2O_4).

3.3. Wettability Test Results

Figure 9 presents the SEM micrographs and EDS analysis of study samples after wettability tests with Al–Si alloys at 900 °C and 2 h as experimental conditions.

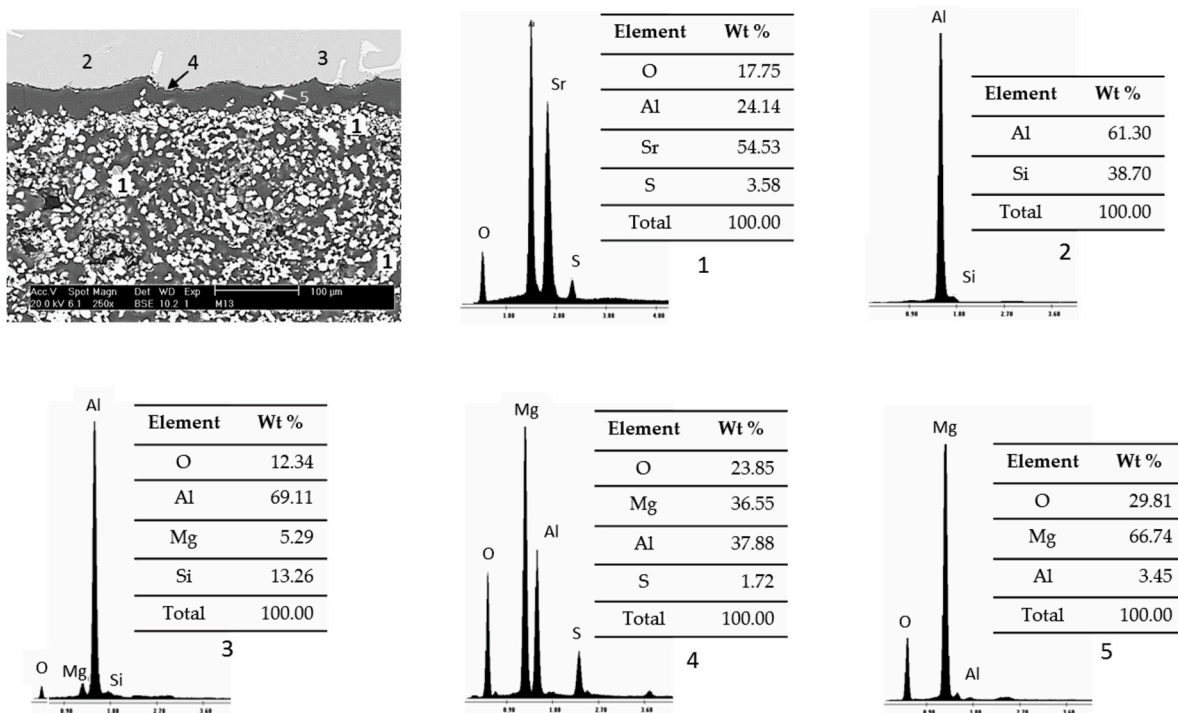


Figure 9. SEM micrograph and EDS spectra of study samples after wettability tests with Al–Si alloys at 900 °C for 2 h as experimental conditions.

According to the percentages of the chemical elements recorded, the particle agglomerates located in the lower area of the micrograph were identified with the number 1 and correspond to the ceramic substrate $\text{Sr}_4\text{Al}_6\text{O}_{12}\text{SO}_4$; the areas identified with numbers 2 and 3 correspond to the Al–Si alloy; reaction products are presented due to the chemical interaction between the ceramic substrate $\text{Sr}_4\text{Al}_6\text{O}_{12}\text{SO}_4$ and the Al–Si alloy, such as a thin line of spinel (MgAl_2O_4) in the boundary with the metal, and identified with the number 4; and isolated sections of magnesium oxide (MgO) are identified with the number 5. Figure 10 shows the mapping via chemical element (SEM) present in the study sample after wettability tests with Al–Si alloys at 900 °C and 2 h as experimental conditions.

The main micrograph (upper left corner) presents the analyzed study sample section. Four main areas are observed: in the lower part, agglomerates of white particles (1); in the upper part, a solid section of dark-gray color (2); attached to the border of Section 2, there is a thin line of products of the reaction (3); and within the metallic zone, there are small light-gray sections (4). According to the distribution of chemical elements, the area identified with the number 1 (agglomerates of light-colored hemispherical particles) corresponds to the ceramic substrate $\text{Sr}_4\text{Al}_6\text{O}_{12}\text{SO}_4$; the dark-gray solid section identified with the number 2 corresponds to the Al–Si alloy; and the line identified with the number 3 corresponds to the spinel (MgAl_2O_4) and magnesium oxide (MgO) phases. The number 4 identifies the presence of manganese and iron intermetallics within the metal alloy, although the latter was not recorded in EDS. On the other hand, strontium diffusion from the ceramic substrate towards the metal alloy, silicon, manganese, and iron from the metal alloy towards the ceramic substrate are observed. The above is the result of the chemical interaction process between the ceramic substrate and the Al–Si alloy (corrosion).

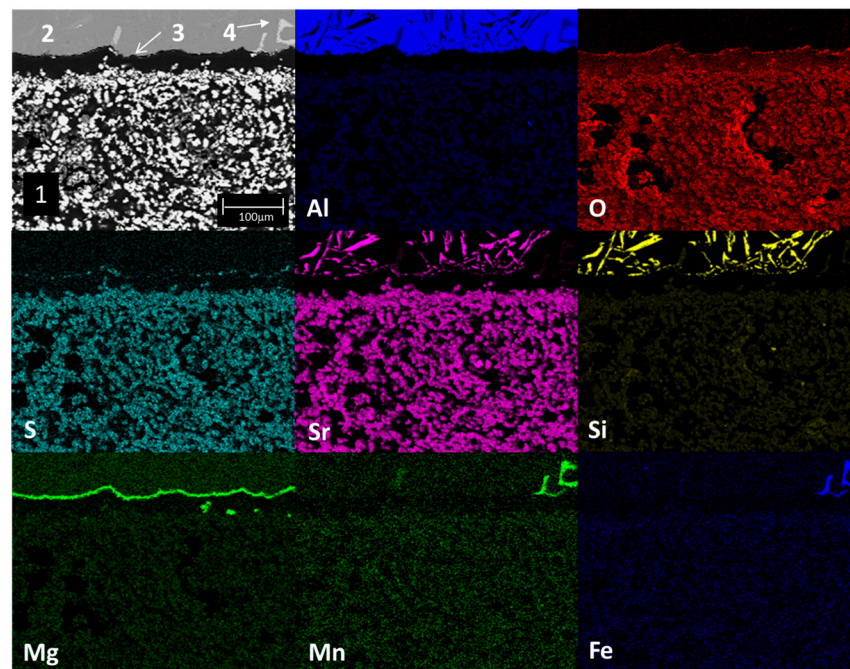


Figure 10. Mapping via chemical element present in the study sample after wettability tests with Al-Si alloys at 900 °C for 2 h as experimental conditions. 1: $\text{Sr}_4\text{Al}_6\text{O}_{12}\text{SO}_4$, 2: Al-Si alloy, and 3–5: reaction products.

Figure 11 presents the SEM micrographs and EDS analysis of study samples after wettability tests with Al-Si alloys at 1000 °C and 2 h as experimental conditions. According to the percentages of the chemical elements recorded, hemispherical and agglomerated particles in the lower part of the micrograph were identified with the number 1 and correspond to the ceramic substrate $\text{Sr}_4\text{Al}_6\text{O}_{12}\text{SO}_4$. The dark-gray solid area identified with the number 2 corresponds to the alloy Al-Si; there are reaction products due to the chemical interaction between the ceramic substrate and the Al-Si alloy, such as a thin line of magnesium oxide (MgO) identified with the number 3 and spinel (MgAl_2O_4) identified with the number 4 on the border with the metal alloy. On the other hand, intermetallics are present in the alloy, formed via Fe and Mn and identified with the number 5.

The above can be corroborated with the chemical element mapping study on the sample after wettability tests with Al-Si alloys at 1000 °C for 2 h as experimental conditions. The results are presented in Figure 12.

The main micrograph (upper left corner) presents the study sample section analyzed using the chemical element mapping (SEM) technique. Four main areas are observed: in the lower part, agglomerates of white particles (1); in the upper part, a solid section of dark-gray color (2); attached to the border of Section 2, there is a thin line of products of the reaction (3); and within the metallic zone there are small light-gray sections (4). According to the distribution of chemical elements, the area identified with the number 1 (agglomerates of light-colored hemispherical particles) corresponds to the ceramic substrate $\text{Sr}_4\text{Al}_6\text{O}_{12}\text{SO}_4$, the dark-gray solid section identified with the number 2 corresponds to the Al-Si alloy, the line identified with the number 3 corresponds to the spinel (MgAl_2O_4) and magnesium oxide (MgO) phases, and with the number 4 the presence of manganese and iron intermetallics is identified within the metal alloy. Strontium diffusion from the ceramic substrate towards the metal alloy, silicon, manganese, and iron from the metal alloy towards the ceramic substrate is observed. The above is the result of the chemical interaction process between the ceramic substrate and the Al-Si alloy (corrosion).

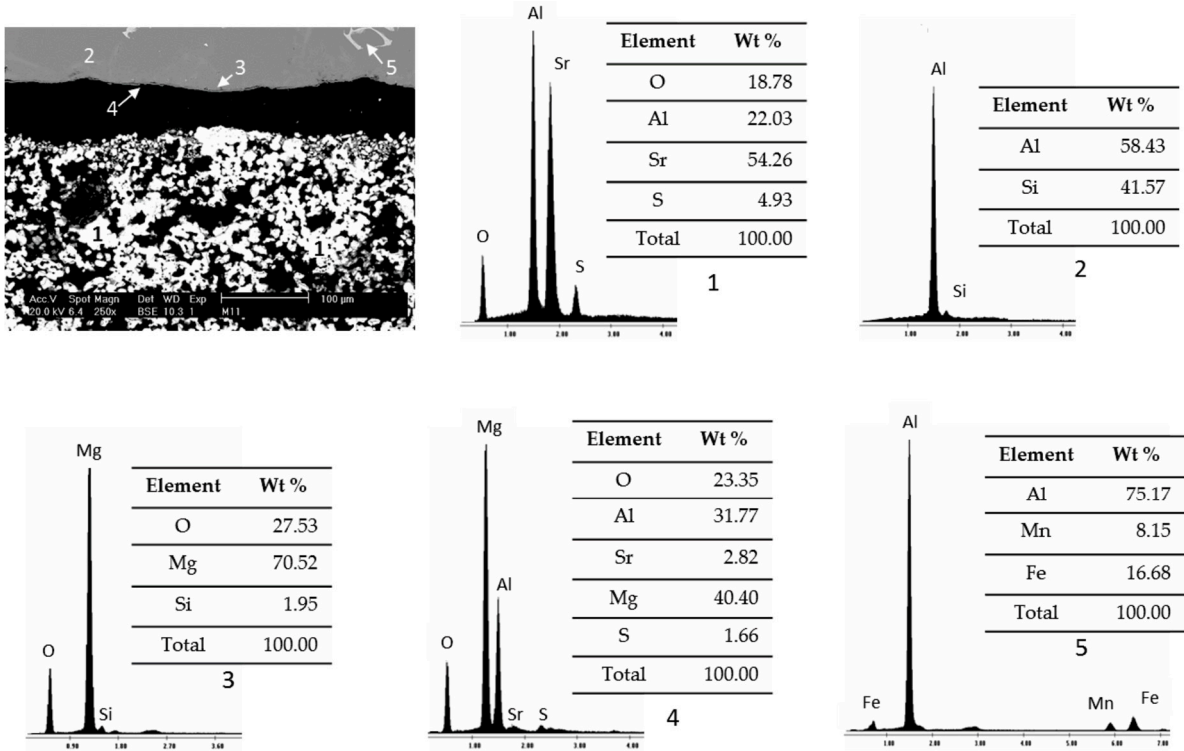


Figure 11. SEM micrograph and EDS spectra of study samples after wettability tests with Al-Si alloys at 1000 °C for 2 h as experimental conditions.

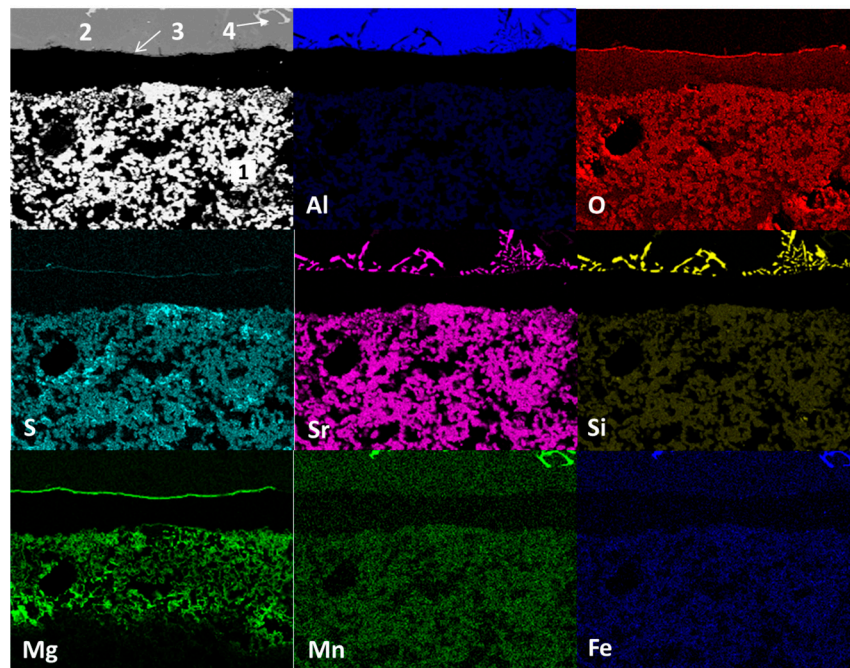


Figure 12. Mapping via chemical element present in the study sample after wettability tests at 1000 °C for 2 h as experimental conditions. 1: $\text{Sr}_4\text{Al}_6\text{O}_{12}\text{SO}_4$, 2: Al-Si alloy, 3: reaction products, and 4: intermetallic.

Figure 13 presents the SEM micrographs and EDS analysis of study samples after wettability tests with Al-Si alloys at 1100 °C and 2 h as experimental conditions.

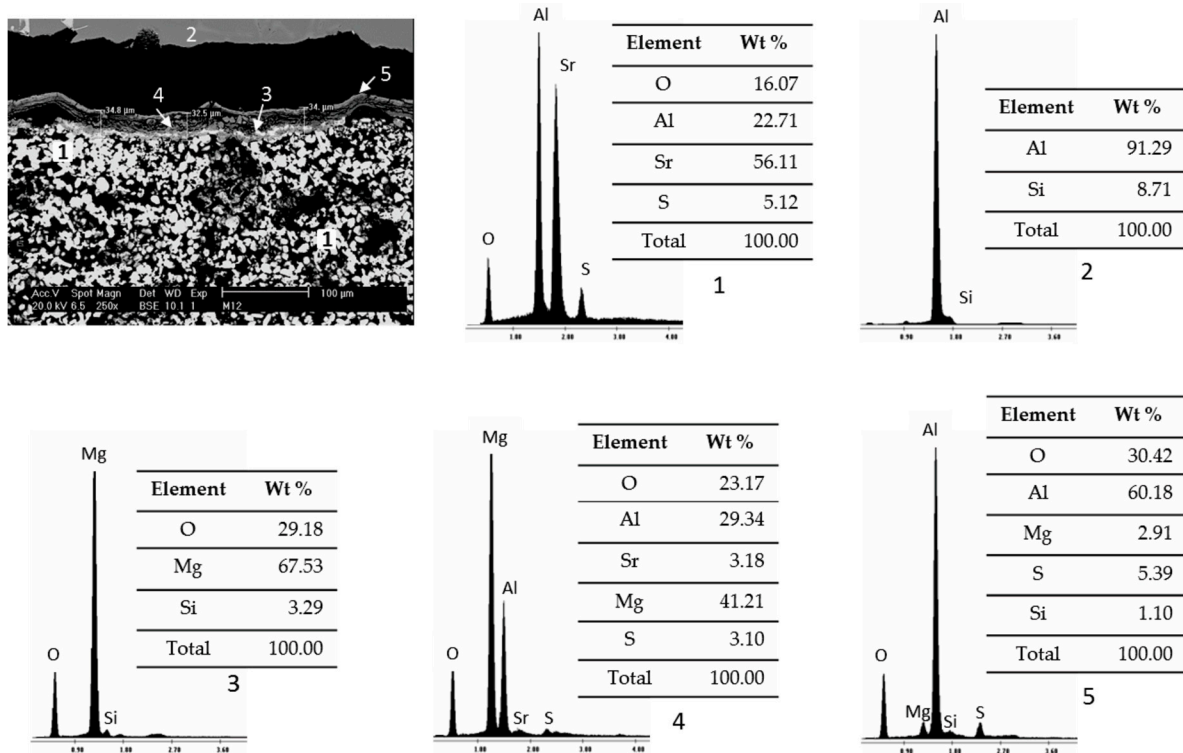


Figure 13. SEM micrograph and EDS spectra of study samples after wettability tests with Al-Si alloys at 1100 °C for 2 h as experimental conditions.

According to the percentages of the chemical elements recorded, hemispherical and agglomerated particles in the lower part of the micrograph were identified with the number 1 and correspond to the ceramic substrate $\text{Sr}_4\text{Al}_6\text{O}_{12}\text{SO}_4$, the dark-gray solid area identified with the number 2 corresponds to the alloy Al-Si, and a reaction zone is observed between the ceramic substrate and the alloy whose thickness has an average value of 34.8 μm with a standard deviation of 1.92%. The products formed are magnesium oxide (MgO), identified with the number 3; spinel (MgAl_2O_4), identified with the number 4; and alumina (Al_2O_3), identified with the number 5. This last reaction product exists in a greater proportion and was only presented at 1100 °C and 2 h as experimental conditions.

The above can be corroborated with the chemical element mapping (SEM) study on the sample after wettability tests with Al-Si alloys at 1100 °C for 2 h as experimental conditions. The results are presented in Figure 14.

The main micrograph (upper left corner) presents the section of the study sample analyzed. Four main zones are observed: in the lower part, agglomerates of white particles (1); in the upper part, a solid section of dark-gray color (2); a zone of reaction products (3); and within the metallic zone there are small light-gray sections (4). According to the distribution of chemical elements, the area identified with the number 1 (agglomerates of light-colored hemispherical particles) corresponds to the ceramic substrate $\text{Sr}_4\text{Al}_6\text{O}_{12}\text{SO}_4$, the dark-gray solid section identified with the number 2 corresponds to the Al-Si alloy, in the lower part of the area identified with number 3, due to the high concentration of magnesium, the presence of magnesium oxide (MgO) was recorded, and a little higher up there is the presence of the spinel phase (MgAl_2O_4).

The rest of the reaction zone and the main product are alumina (Al_2O_3). The number 4 identifies the presence of manganese and iron intermetallics within the metal alloy, although these phases were not recorded in the EDS analyses. On the other hand, the strontium and sulfur diffusion from the ceramic substrate towards the metal alloy, silicon, manganese, and iron from the metal alloy towards the ceramic substrate are observed. This reaction results from the chemical interaction between the ceramic substrate and the Al-Si alloy (corrosion).

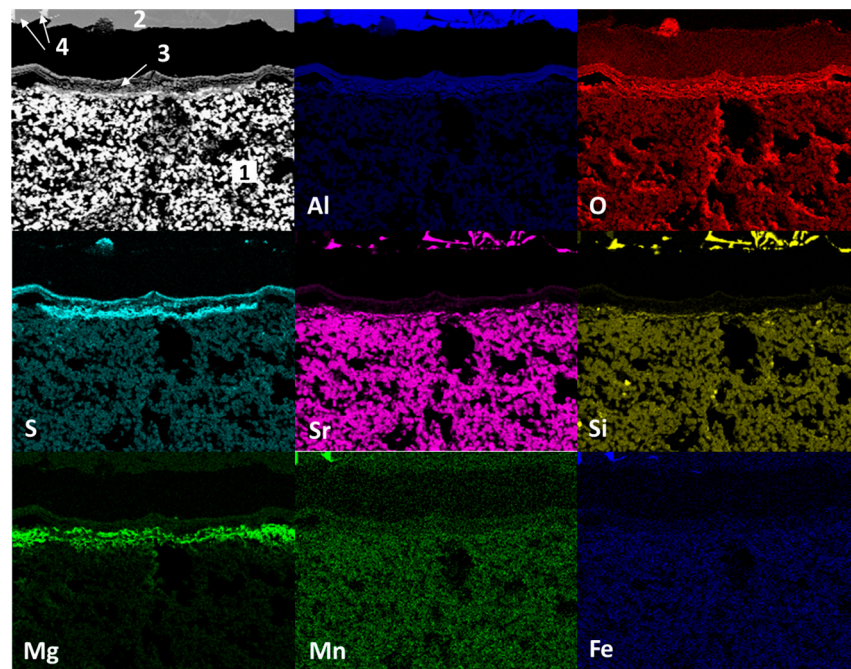


Figure 14. Mapping via chemical element present in the study sample after wettability tests at 1100 °C for 2 h as experimental conditions. 1: $\text{Sr}_4\text{Al}_6\text{O}_{12}\text{SO}_4$, 2: Al–Si alloy, 3: reaction products, and 4: intermetallics.

Figure 15 presents the results referring to the wetting angles recorded in the wettability tests of samples tested at 900, 1000, and 1100 °C for 2 h in contact with Al–Si alloys as experimental conditions.

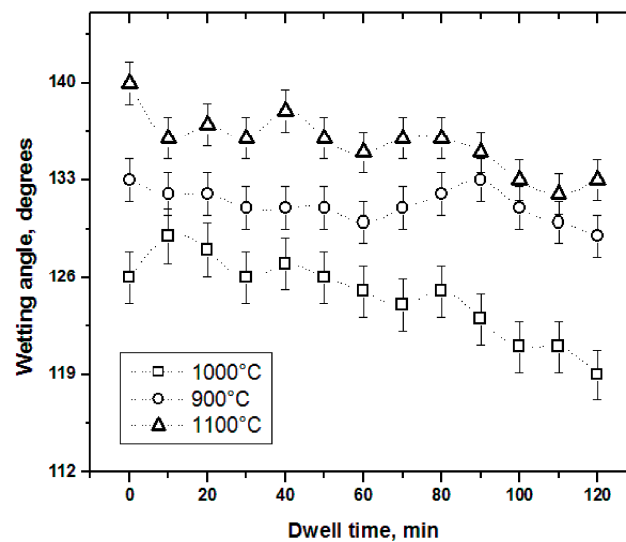


Figure 15. Wetting angles of samples tested at 900, 1000, and 1100 °C with different isotherms and in contact with Al–Si alloys as experimental conditions.

As a first analysis, it is worth highlighting that all data are graphed within the zone of non-wettable materials (above 90°) in the three samples. On the other hand, the variation of the wetting angles can be observed with respect to the increase in test time. The sample exposed to 1100 °C recorded the highest average wetting angle (≈135.61°), which means that it is the sample with the least affection by the liquid metal in the tests. This behavior may be due to the formation of a considerable layer of reaction products on the surface of the ceramic substrate, consisting mainly of alumina of around 35 μm thickness, which acts

as a protective shield for the sample and prevents the rest of the material from corrosion. The samples at 900 °C and 1000 °C presented very thin layers of reaction products, mainly spinel, less than 5 µm thick. The sample tested at 1000 °C reported the lowest average wetting angle ($\approx 124.57^\circ$).

4. Conclusions

- In general, when carrying out the static immersion tests, the performance of the $\text{Sr}_4\text{Al}_6\text{O}_{12}\text{SO}_4$ ceramic substrate can be highlighted since, despite the extreme conditions (1000 °C for 100 h) to which it was subjected, the corrosion layer on the samples was less than 100 µm, which makes the compound resistant to corrosion due to the alloys used;
- There are diffusion phenomena of chemical elements between the ceramic substrate and the aluminum alloy, which are a function of temperature;
- Furthermore, reported reaction products mainly contain alumina (Al_2O_3), magnesium oxide (MgO), and spinel (MgAl_2O_4). These compounds form a surface layer protecting the sample from chemical attack by liquid aluminum;
- These results suggest the use of the ceramic substrate $\text{Sr}_4\text{Al}_6\text{O}_{12}\text{SO}_4$ in the refractory industry, possibly as an additive to commercial refractory ceramics;
- For future work, carrying out the same study with the aluminum–magnesium alloy and as an additive in commercial refractory ceramics is considered prudent.

Author Contributions: Conceptualization, J.A.R.-G. and E.R.-R.; methodology, J.A.R.-G., C.A.C.-A., and E.R.-R.; formal analysis, all authors; investigation, all authors; writing—original draft preparation, J.A.R.-G.; writing—review and editing, J.A.R.-G., C.A.C.-A., and R.D.L.-G. All authors have read and agreed to the published version of the manuscript.

Funding: This research received no external funding.

Institutional Review Board Statement: The study was conducted in accordance with the Declaration of Helsinki, and approved by the Institutional Review Board of Universidad Politécnica de Victoria (protocol code RD-023 and 1 July 2023).

Informed Consent Statement: Not applicable.

Data Availability Statement: Data in this study are available upon request with justification.

Conflicts of Interest: The authors declare no conflicts of interest.

References

1. Reddy, P.S.; Reddy, N.G.; Serjun, V.Z.; Mohanty, B.; Das, S.K.; Reddy, K.R.; Rao, B.H. Properties and Assessment of Applications of Red Mud (Bauxite Residue): Current Status and Research Needs. *Waste. Biomass. Valori.* **2020**, *12*, 1185–1217. [[CrossRef](#)]
2. Ujaczki, É.; Feigl, V.; Molnár, M.; Cusack, P.; Cutin, T.; Courtney, R.; O'Donoghue, L.; Davris, P.; Hugi, C.; Evangelou, M.W.H.; et al. Re-using bauxite residues: Benefits beyond (critical raw) material recovery. *J. Chem. Technol. Biotechnol.* **2018**, *93*, 2498–2510. [[CrossRef](#)]
3. Verma, A.S.; Suri, N.M.; Kant, S. Applications of bauxite residue: A mini-review. *Waste Manag. Res.* **2017**, *35*, 999–1012. [[CrossRef](#)]
4. Evans, K. The History, Challenges, and New Developments in the Management and Use of Bauxite Residue. *J. Sustain. Metall.* **2016**, *2*, 316–331. [[CrossRef](#)]
5. Jones, B.E.H.; Haynes, R.J. Bauxite Processing Residue: A critical Review of its Formation, Properties, Storage, and Revegetation. *Crit. Rev. Env. Sci. Technol.* **2011**, *41*, 271–315. [[CrossRef](#)]
6. Oliveira, M.; Agathopoulos, S.; Ferreira, J.M. Reactions at the interface between Al_2O_3 - SiO_2 ceramics with additives of alkaline-earth oxides and liquid Al-Si alloy. *J. Mater. Res.* **2002**, *17*, 641–647. [[CrossRef](#)]
7. George, E.T.; Mackenzie, D.S. *Handbook of Aluminum: Alloy Production and Materials Manufacturing*, 1st ed.; CRC Press: Boca Raton, FL, USA, 2003; pp. 1–115.
8. Rahaman, M.N. *Ceramic Fabrication Processes: An Introductory Overview Processing and Sintering*, 2nd ed.; CRC Press: Boca Raton, FL, USA, 2003; pp. 1–48.
9. López-Perales, J.F.; Contreras, J.E.; Vázquez-Rodríguez, F.J.; Gómez-Rodríguez, C.; Díaz-Tato, L.; Banda-Muñoz, F.; Rodríguez, E.A. Partial replacement of a traditional raw material by blast furnace slag in developing a sustainable conventional refractory castable of improved physical-mechanical properties. *J. Clean. Prod.* **2021**, *306*, 127266. [[CrossRef](#)]

10. Chen, J.; Zhao, H.; Yu, J.; Zhang, H.; Li, Z.; Zhang, J. Synthesis and characterization of reaction-bonded calcium aluminium-titanate-bauxite-SiC composite refractories in a reducing atmosphere. *Ceram. Int.* **2018**, *44*, 15338–15345. [[CrossRef](#)]
11. Yurkov, A.L.; Pikhutin, I.A. Corrosion of aluminosilicate refractories by molten aluminum and melts based upon it in melting and casting units. *Ref. Ind. Ceram.* **2009**, *50*, 212–219. [[CrossRef](#)]
12. Pereira, A.L.; Reis, M.A.; Ferreira, L.L.H.C.; Nakachima, P.M. Brazilian refractory grade bauxite: A new alternative to refractories makers and users. *Ceramic* **2019**, *65*, 40–46. [[CrossRef](#)]
13. Santos, D.P.; Pelissari, P.I.B.G.B.; de Oliveira, B.S.; Leiva, D.R.; de Mello, R.F.; Pandolfelli, V.C. Materials selection of furnace linings with multi-component refractory ceramics based on an evolutionary screening procedure. *Ceram. Int.* **2020**, *46*, 4113–4125. [[CrossRef](#)]
14. Verran, G.O.; Kurzawa, U. An experimental study of aluminum can recycling using fusion in induction furnace. *Res. Conserv. Recycl.* **2008**, *52*, 731–736. [[CrossRef](#)]
15. Bonadia, P.; Valenzuela, F.A.O.; Bittencourt, L.R.; Pandolfelli, V.C. Aluminosilicates refractories for aluminum cell linings. *Am. Ceram. Soc.* **2005**, *84*, 26–31.
16. Moore, R.E. *Refractories, Structure and Properties of*, 2nd ed.; Elsevier: Amsterdam, The Netherlands, 2001; pp. 8079–8087.
17. Sangghaleh, A.; Mohammad, H. An investigation on the wetting of polycrystalline alumina by aluminium. *J. Mat. Proc. Technol.* **2008**, *197*, 156–160. [[CrossRef](#)]
18. Allaire, C.; Desclaux, P. Effect of Alkalies and of a reducing atmosphere on the corrosion of refractories by molten aluminum. *J. Am. Ceram. Soc.* **1991**, *74*, 2781–2785. [[CrossRef](#)]
19. Ibarra, M.N.; Almanza, J.M.; Cortés, D.A.; Escobedo, J.C.; Torres, J. The effect of SrSO₄ and BaSO₄ on the corrosion and wetting by molten aluminum alloys of mullite ceramics. *Ceram. Int.* **2010**, *36*, 1205–1210. [[CrossRef](#)]
20. Adabifiroozjaei, E.; Koshy, P.; Sorrell, C. Effects of AlPO₄ addition on the corrosion resistance of andalusite-based low-cement castables with molten Al-alloy. *J. Eur. Ceram. Soc.* **2013**, *33*, 1067–1075. [[CrossRef](#)]
21. Ibarra, M.N.; Almanza, J.M.; Cortés, D.A.; Escobedo, J.C.; Pech, M.; Martínez, J. Effect of the addition of alkaline earth sulfates to mullite ceramics on the corrosion and wetting by Al-Mg alloy. *J. Eur. Ceram. Soc.* **2015**, *35*, 2189–2194. [[CrossRef](#)]
22. Adabifiroozjaei, E.; Koshy, P.; Pardehkhorrām, R.; Rastkerdar, E.; Sorrell, C. Interfacial reactions between BaAl₂Si₂O₈ and molten Al alloy at 850 °C. *J. Am. Ceram. Soc.* **2015**, *98*, 3299–3307. [[CrossRef](#)]
23. Rodríguez, J.A.; Ríos, E.; Rocha, E.; Almanza, J.M.; Torres, J.; Refugio, E. Kinetics of formation and crystal structure determination of Sr₄Al₆O₁₂SO₄. *Mater. Res.* **2016**, *19*, 125–132. [[CrossRef](#)]
24. Storoshenko, M.S.; Umanskyi, O.P.; Terentiev, O.; Krasovkyy, V.P.; Martzenyuk, I.S.; Gubin, Y. Contact interaction of chromium diboride with iron-based self-fluxing alloy. *Powder Metall. Met. Ceram.* **2023**, *61*, 465–473. [[CrossRef](#)]
25. Xiaoyan, C.; Zhihui, L.; Yanjie, Z.; Chengkang, Q.; Shurong, L.; Fei, L. Wetting and interfacial phenomena between a Ni-based superalloy and silica-based ceramic cores with ZrSiO₄ additions. *J. Phys. Conf. Ser.* **2024**, *2671*, 012025.
26. Rodríguez, J.A.; Rocha, E.; Torres, J.; Almanza, J.M. Synthesis by solid state reaction of the Sr₄Al₆O₁₂SO₄ compound. *J. Ceram. Process. Res.* **2011**, *12*, 310–313.
27. Sangghaleh, A.; Halali, M. Effect of magnesium addition on the wetting of alumina by aluminium. *Appl. Surf. Sci.* **2009**, *255*, 8202–8206. [[CrossRef](#)]

Disclaimer/Publisher’s Note: The statements, opinions and data contained in all publications are solely those of the individual author(s) and contributor(s) and not of MDPI and/or the editor(s). MDPI and/or the editor(s) disclaim responsibility for any injury to people or property resulting from any ideas, methods, instructions or products referred to in the content.